nature communications

Article

https://doi.org/10.1038/s41467-025-63385-3

Inequality in human exposure to future climate extremes

Received: 10 September 2024

Accepted: 15 August 2025

Published online: 28 August 2025

Check for updates

Parisa Hosseinzadehtalaei[1] ✉, Rafiq Hamdi[1,2], Hamid Moradkhani[3,4], Piet Termonia[1,2] & Hossein Tabari[2,5,6] ✉

Future climate extremes are expected to worsen existing inequalities in human exposure, yet the specific disparities across income groups are not well understood. We investigate how future floods, heatwaves, droughts, and compound hot-dry events will impact high- and low-income countries under various shared socioeconomic pathways (SSPs). We find that low-income countries are projected to experience more severe exposure to these events, primarily due to accelerated population growth rather than climate change. Exposure inequality between high- and low-income countries decreases as event severity increases, with the effects of population growth diminishing and the impact of climate change becoming more pronounced. While compound hot-dry events have a greater overall impact compared to single events, the inequality in exposure to these events is less pronounced. These findings underscore the need for targeted adaptation strategies that address both demographic drivers and the spatial-temporal dynamics of extreme events to effectively manage socioeconomic risks.

Extreme weather events driven by human-induced global warming are increasingly threatening human well-being[1–3], with the most devastating effects occurring in the world's lowest-income regions[4,5]. According to the Global Climate Risk Index 2021[6], eight of the ten countries most affected by climate extremes in 2019 were lower-middle-income nations. Low-income countries face amplified risks from heatwaves, droughts, and floods due to inadequate infrastructure, limited access to essential services, the absence of multi-hazard early warning systems, and ineffective disaster risk reduction strategies, all of which hinder their ability to prepare for and recover from such disasters[7–13]. These shortcomings result in severe damage and prolonged suffering when disasters strike[14]. Acknowledging these disparities, the 27th Conference of the Parties to the United Nations Framework Convention on Climate Change (COP27) reached an agreement to establish a fund to compensate vulnerable developing countries for losses and damages caused by extreme climate events[15]. This agreement represents a crucial step in addressing the disproportionate impacts of climate change on the world's lowest-income communities and underscores the urgent need for global cooperation and support.

Extreme events are projected to become more frequent and intense with changing climatic patterns worldwide[16–19], escalating the already formidable adaptation costs for low-income countries in the coming decades[15,20–22]. While studies have addressed future exposure inequality for heatwaves and droughts[23–25], less attention has been given to floods[22,26] and compound extremes[27]. Key knowledge gaps remain in understanding the disparities in human exposure to these events between low- and high-income countries.

First, the drivers of exposure inequality have not been systematically analyzed, limiting insights into how socioeconomic and demographic factors, such as population growth, interact with climate change to exacerbate disparities. Second, while compound events

[1]Department of Physics and Astronomy, Ghent University, Ghent, Belgium. [2]Department of Meteorological and Climate Research, Royal Meteorological Institute of Belgium, Uccle, Belgium. [3]Department of Civil, Construction and Environmental Engineering, The University of Alabama, Tuscaloosa, AL, USA. [4]Center of Complex Hydrosystems Research, The University of Alabama, Tuscaloosa, AL, USA. [5]Faculty of Applied Engineering, University of Antwerp, Antwerp, Belgium. [6]United Nations University Institute for Water, Environment and Health (UNU-INWEH), Richmond Hill, ON, Canada.
✉e-mail: parisa.hosseinzadehtalaei@ugent.be; hossein.tabari@uantwerpen.be

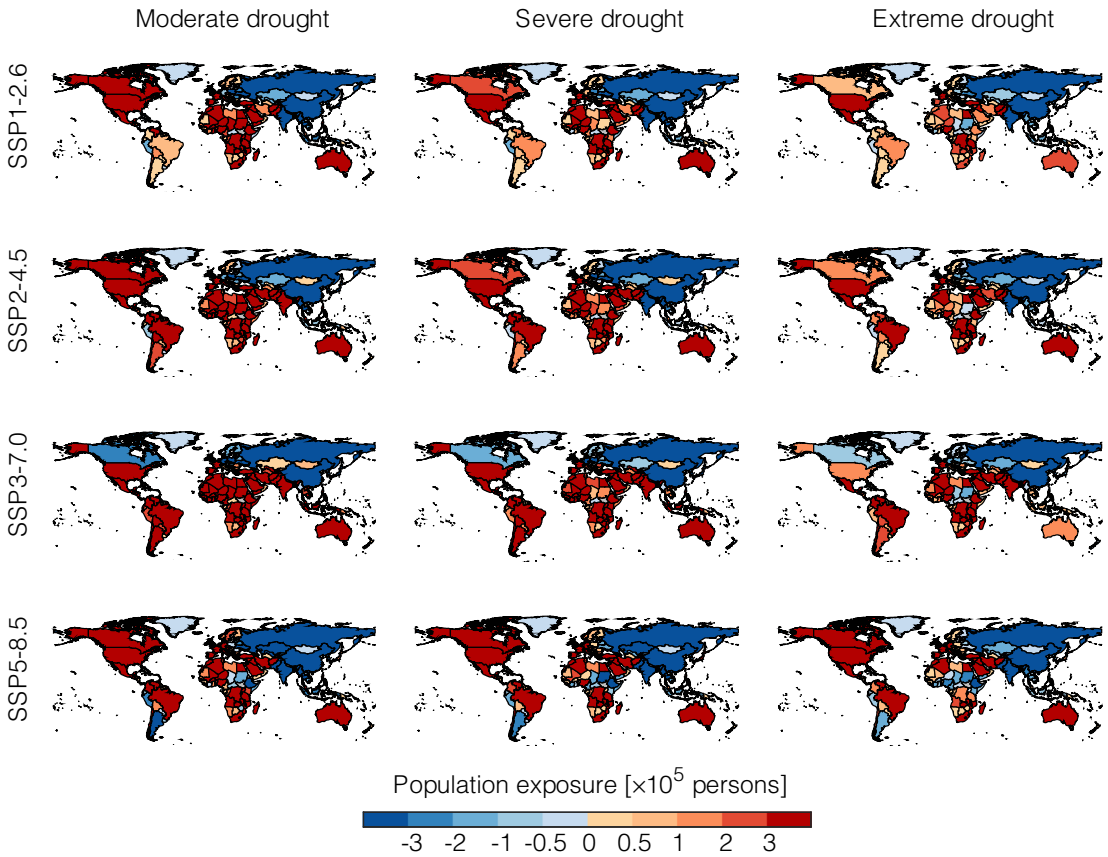

Fig. 1 | Projected changes in population exposure to moderate, severe, and extreme drought under different scenarios for the end of the twenty-first century. The changes are computed by comparing the late twentieth century and the late twenty-first century.

often result in more severe impacts than individual extremes[27,28], differences in projected exposure inequalities between these event types remain underexplored. Third, comparative analyses of inequality across multiple extreme event types are limited. Finally, the relationship between the severity of climate extremes and exposure inequality requires further investigation to design equitable adaptation strategies. This study addresses these gaps by examining how future individual and compound extreme events of varying severities, under different socioeconomic and emission scenarios, might unequally impact low- and high-income countries.

Specifically, we explore the disparities in human exposure to projected floods, heatwaves, droughts, and compound hot-dry events between low- and high-income countries, categorized according to World Bank income groups based on gross national income (GNI) per capita. Exposure inequality is defined as the difference in projected changes in population exposure between low- and high-income countries (see the "Methods" section). Our analysis is based on the assumption that high-income regions, with their stronger institutional and individual capacities, will be better able to adapt to warming trends compared to low-income regions. To quantify heatwaves, droughts, and compound hot-dry events, we use 26 global climate models (GCMs) from the Coupled Model Intercomparison Project Phase 6 (CMIP6[29]) ensemble across four shared socioeconomic pathway (SSP) scenarios. Floods are assessed using a 28-member ensemble of seven global hydrological models (GHMs) forced by four GCMs: CLM4.5[30], H08[31], JULES-W1[32], LPJmL[33], MATSIRO[34], ORCHIDEE[35], and WaterGAP2[36]. Each GHM was driven by three state-of-the-art, observation-based historical climate datasets: GSWP3[37], PGFv2[38], and WFD/WFDEI[39]. Our analysis reveals that the lowest-income countries face disproportionate exposure to future floods, heatwaves, droughts, and compound hot-dry events. This inequality is primarily driven by accelerated population growth in low-income countries rather than climate change. While compound extreme events have a greater overall impact, the inequality in human exposure to these events is anticipated to be less pronounced compared to individual drought events. Therefore, to effectively develop disaster risk reduction strategies and mitigate the increasing socioeconomic risks of extreme events in a changing climate, it is crucial to systematically analyze the spatial and temporal interactions among different types of extreme events, their severity, economic development, and demographic changes.

Results

Population exposure

We assessed future changes in population exposure to floods, heatwaves, droughts, and compound hot-dry events, which are defined as the product of population and the likelihood of these events at each grid cell (see the "Methods" section). This analysis was conducted under various SSPs, which outline potential trajectories for global societal, demographic, and economic development, including factors such as technological progress, energy use, and environmental policies[40]. Exposure was evaluated across three severities for each event type: moderate, severe, and extreme. Our results indicate that population exposure to extreme events is projected to rise in most countries (Fig. 1 and Supplementary Figs. 1–3). Specifically, exposure to floods, heatwaves, droughts, and compound hot-dry events is expected to increase in 71–83%, 99–100%, 59–74%, and 83–91% of global countries, respectively, depending on the scenario and event severity. For all four event types, population exposure grows with event severity under all future scenarios. Among these, the increase in

https://doi.org/10.1038/s41467-025-63385-3

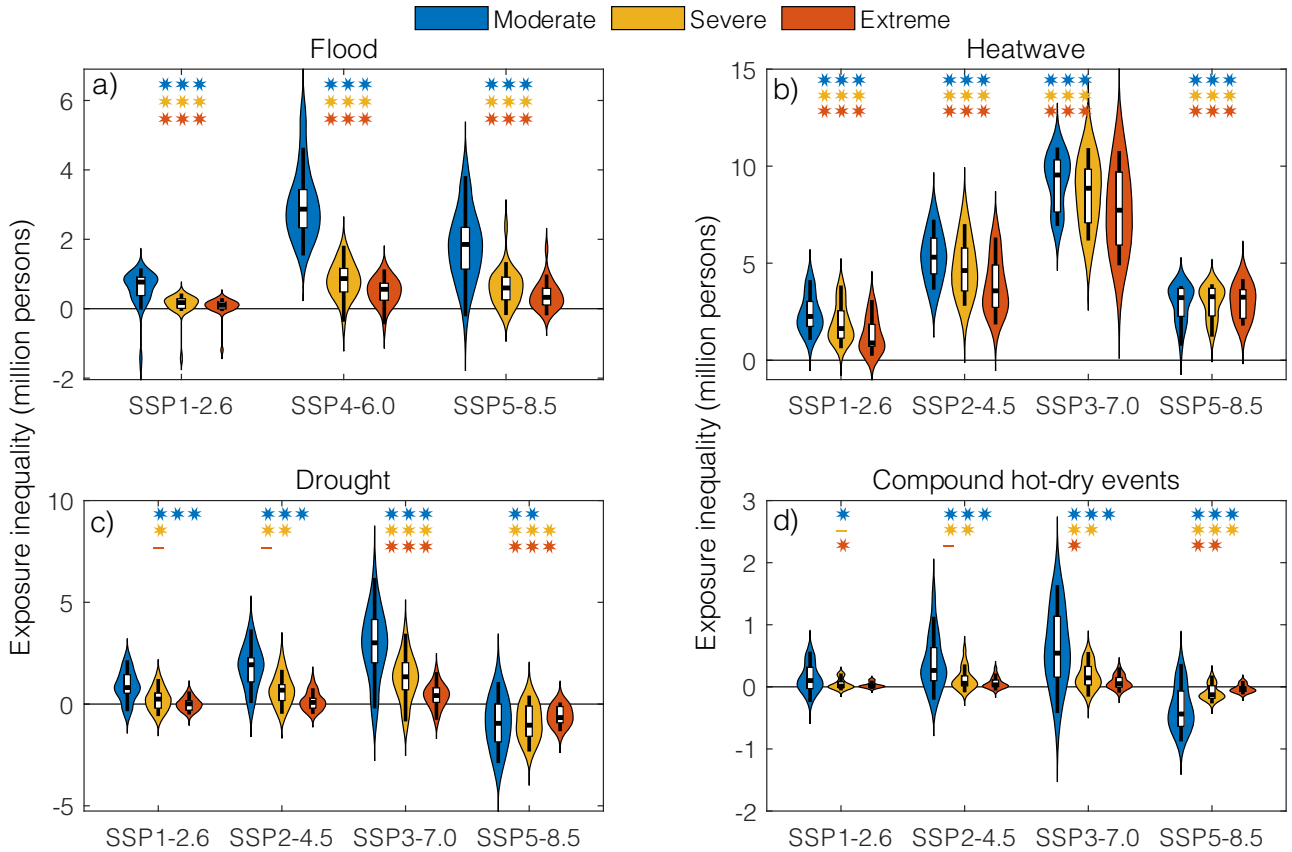

Fig. 2 | Inequality in projected changes in population exposure to extreme events of different severities across various future scenarios. The plots show the difference in projected changes in population exposure to extreme events between low- and high-income countries, with positive values indicating higher exposure in low-income countries. Violin plots depict the ensemble probability density, with $n = 28$, 18, 22, and 22 ensemble members used for **a** flood, **b** heatwave, **c** drought, and **d** compound events, respectively. Box plots within the violins show the median (horizontal black line), the interquartile range (IQR) from the 25th to 75th percentile (box), and whiskers extending to the most extreme data points within 1.5 × IQR from the box. Statistical significance was calculated using the two-sided Wilcoxon rank-sum test, with "✱✱✱," "✱✱," and "✱" indicating significant inequality at the 1%, 5%, and 10% levels, respectively, while "–" indicates no significance. The changes are computed by comparing the late twentieth century and the late twenty-first century.

population exposure is most widespread and pronounced for heatwaves and compound hot-dry events.

Inequality in population exposure

After analyzing country-level population exposure to extreme events, exposure inequality was assessed between low- and high-income countries (Supplementary Fig. 4). Notable exposure inequality is observed across various extreme events, severities, and future scenarios, except for SSP5 in the cases of drought and compound hot-dry events (Fig. 2). The magnitude and statistical significance of exposure inequality, however, vary by type of extreme event, SSP scenario, and severity.

Among the four types of extreme events, heatwaves exhibit the largest exposure inequality, while compound hot-dry events have the smallest (Fig. 2). Inequality in population exposure to floods and heatwaves across varying severities and scenarios is statistically significant at the 1% level. For droughts, differences in projected exposure between low- and high-income countries are statistically significant at levels between 10% and 1% for moderate and severe events across all scenarios, while for extreme droughts, they are statistically significant only under SSP3 and SSP5, both at the 1% level. In the case of compound hot-dry events, differences in projected exposure are statistically significant at levels between 10% and 1% across all cases, except for severe events under SSP1 and extreme events under SSP2.

The results indicate that exposure inequality generally decreases as event severity increases (Fig. 2). For instance, for floods, exposure inequality for moderate floods is about six times larger than for extreme floods and four times larger than for severe floods. Specifically, for moderate and severe events, low-income countries experience disproportionately higher exposure compared to high-income countries, while this relative inequality diminishes for extreme events.

Exposure inequality also differs across SSP scenarios (Fig. 2). The highest inequality is observed under SSP3, which reflects slower socioeconomic development and limited climate action[41]. In contrast, the lowest inequality occurs under SSP1, which prioritizes sustainable and inclusive development[41], leading to a more equitable distribution of exposure. For example, for heatwaves, exposure inequality for SSP3 is 4–9 times (depending on event severity) larger than for SSP1. These findings underscore the role of socioeconomic pathways in shaping exposure inequality and emphasize the potential for equitable development strategies to reduce disparities in vulnerability to extreme events.

Comparison of exposure inequality between individual and compound extreme events

The increasing occurrence and impacts of compound extreme events[42,43] underscore the importance of comparing population exposure and its inequality between drought and compound hot-dry events. Our findings reveal that the projected population exposure to compound hot-dry events is more pronounced than that of individual drought events (Fig. 3), consistent with previous studies[27,28]. However, when considering inequality in population exposure between low- and

https://doi.org/10.1038/s41467-025-63385-3

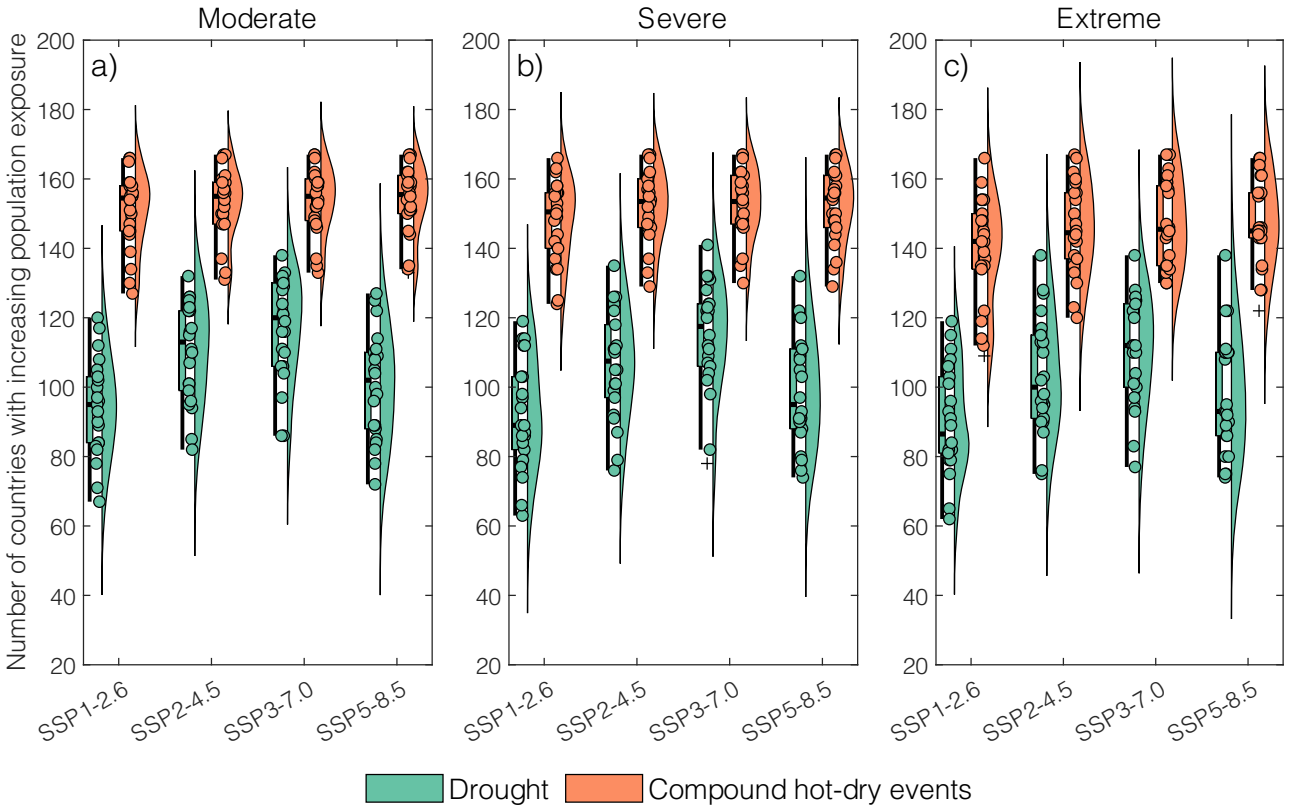

Fig. 3 | Comparison of population exposure to drought and compound hot-dry events. The plots display the number of countries with increased population exposure to **a** moderate, **b** severe, and **c** extreme drought and compound hot-dry events. Violin plots represent the ensemble probability density, $n = 22$ ensemble members. Dots represent results from individual climate models. Box plots show the median (horizontal black line), the interquartile range (IQR) from the 25th to 75th percentile (box), and whiskers extending to the most extreme data points within 1.5 × IQR from the box.

high-income countries, drought exhibits higher inequality than compound hot-dry events (Fig. 2). Except for SSP5, where no inequality is observed for either individual or compound events, the exposure inequality for drought is, on average, eight times larger than for compound hot-dry events for moderate, severe, and extreme events, respectively. The disparity between the two types of events decreases as event severity increases. The smaller exposure inequality for compound hot-dry events stems from their more widespread global impacts, which reduce relative differences between low- and high-income countries. Over 83% of countries globally are projected to experience increased population exposure to compound hot-dry events. In contrast, only 47–70% of countries are projected to see increased exposure to drought, with impacts concentrated more heavily in low-income countries (Fig. 3).

Drivers of exposure inequality

To understand the driving factors behind this exposure inequality, we conducted a contribution analysis (see the "Methods" section). In most cases, population growth is the primary factor driving exposure inequality, with its impact diminishing as the extremity of the events increases (Fig. 4). For floods, both climate change and population growth contribute to the exposure inequality. In SSP1 and SSP4, population changes contribute considerably more than climate change (46–76% for population vs. less than 34% for climate change). Conversely, in SSP5, the effect of climate change surpasses that of population growth. For other types of extreme events, population growth and climate change have opposing impacts on exposure inequality: population growth increases the inequality, while climate change decreases it. Specifically, the contribution of population growth to exposure inequality for heatwaves based on the ensemble median is 54–81% for moderate, 46–75% for severe, and 19–40% for extreme events, depending on the scenario, whereas climate change has an opposing effect of up to 75%. For droughts, population growth accounts for 53–82% of the exposure inequality for moderate events, 48–77% for severe events, and 46–75% for extreme events. The contribution of population growth drops to below 16% for the exposure inequality to compound hot-dry events. Overall, our results indicate that while changes in population exposure to extreme events are influenced by both climate and population changes, the exposure inequality between low- and high-income countries is predominantly driven by population growth.

To better understand the factors driving exposure inequality to extreme events, we compared the impacts of climate change (Fig. 5) and population growth (Fig. 6) between low-income and high-income countries. For drought and compound hot-dry events, climate change impacts are substantially larger in high-income countries (Figs. 5 and S5–S8). In contrast, for floods and heatwaves, climate change signals are generally larger in low-income countries; however, these signals are mostly insignificant (Figs. 5 and S5–S8).

Population growth in low-income countries is projected to be substantially higher than in high-income countries across all SSP scenarios, except after 2060 under SSP5 (Fig. 6). The differences in population growth between low- and high-income countries are statistically significant at the 1% level across all scenarios, with the largest disparities observed under SSP3 and SSP4, and the smallest under SSP1 and SSP5. These differences are expected to grow toward the end of the century, with the sharpest increases occurring under SSP3 and SSP4. In SSP5, higher population growth in high-income countries after 2060 is driven by high fertility rates, supported by advanced technological progress, very high living standards, and factors such as improved work-

https://doi.org/10.1038/s41467-025-63385-3

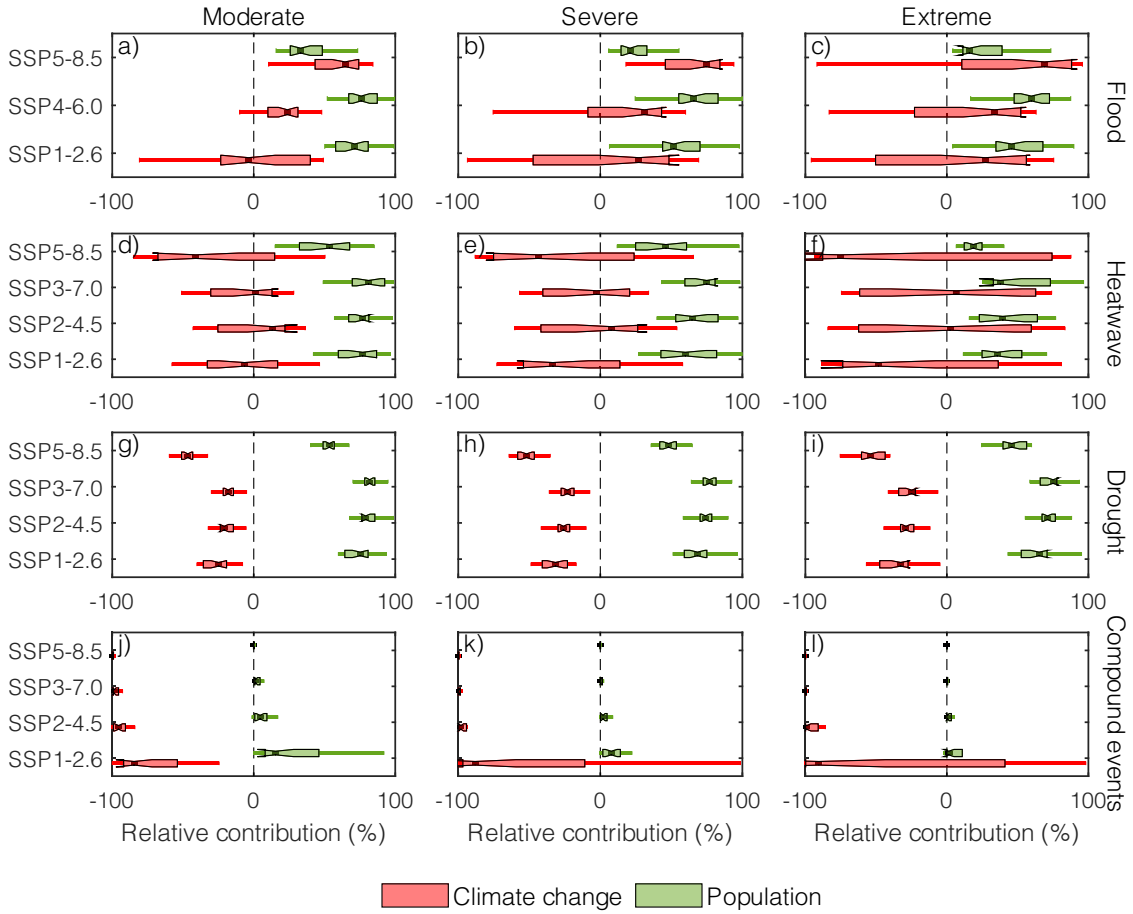

Fig. 4 | Relative contributions of climate change and population growth to projected changes in population exposure to extreme events between low- and high-income countries. Results for floods (**a** moderate; **b** severe; **c** extreme), for heatwaves (**d** moderate; **e** severe; **f** extreme), for droughts (**g** moderate; **h** severe; **i** extreme), and for compound hot-dry events (**j** moderate; **k** severe; **l** extreme). Box plots show the median (vertical black line), the interquartile range (IQR; box), and whiskers extending to the most extreme data points within 1.5 × IQR. The number of ensemble members is $n = 28$ for floods, $n = 18$ for heatwaves, $n = 22$ for droughts, and $n = 22$ for compound events.

family balance and increased use of immigrant domestic assistants[44]. Despite this, during the early decades of the twenty-first century, population growth will likely remain higher in lower-income countries due to higher birth rates and younger populations.

The results in Figs. 5 and 6 confirm the findings in Fig. 4, demonstrating that population growth is the main driver of inequality in human exposure to climate extremes. For drought and compound hot-dry events, while climate change signals are notably larger in high-income countries, higher population growth in low-income countries counterbalances this pattern, resulting in disproportionately higher human exposure in low-income countries. For floods and heatwaves, climate change signals are larger in low-income countries but not statistically significant; this is further amplified by substantially higher population growth in these countries, resulting in substantially greater exposure in low-income countries.

Discussion

Extreme weather events have intensified substantially due to climate change, with rising global temperatures having led to more severe and frequent floods, heatwaves, droughts, and compound extreme events[45–48]. Climate models project a continued increase in the frequency and severity of these events[49–52], making it crucial to understand their impacts across different economic stratifications for effective adaptation and resilience strategies, ensuring support reaches the populations most at risk.

Our analysis of inequality in exposure to floods, heatwaves, droughts, and compound hot-dry events reveals that individuals in lower-income countries face greater exposure compared to those in wealthier nations. In food-deficit, low-income countries, the social consequences of climate extremes are particularly severe due to reliance on subsistence agriculture and primary sector activities, which make food security highly vulnerable to climate shocks[53]. This vulnerability is further exacerbated by weak governance, ineffective market systems, and insufficient food aid, leading to famine, potential conflicts over scarce resources, and increased mortality rates. These factors trap countries in a cycle of poverty and instability, hindering recovery and adaptation[54].

This disparity in exposure to extreme events is driven more by population growth than climate change (Fig. 4). Low-income countries are expected to have substantially higher population growth rates, leading to more people living in vulnerable areas. Although this study focuses on the latter part of the twenty-first century, lower-income countries with higher fertility rates will have a younger population[55], meaning many will face climate risks throughout their lives.

We found that the impact of population growth on exposure inequality decreases as the severity of extreme events increases. This is because more extreme events exhibit larger changes due to climate change compared to less severe events, which amplifies the negative impacts of climate change on inequality and reduces the relative

https://doi.org/10.1038/s41467-025-63385-3

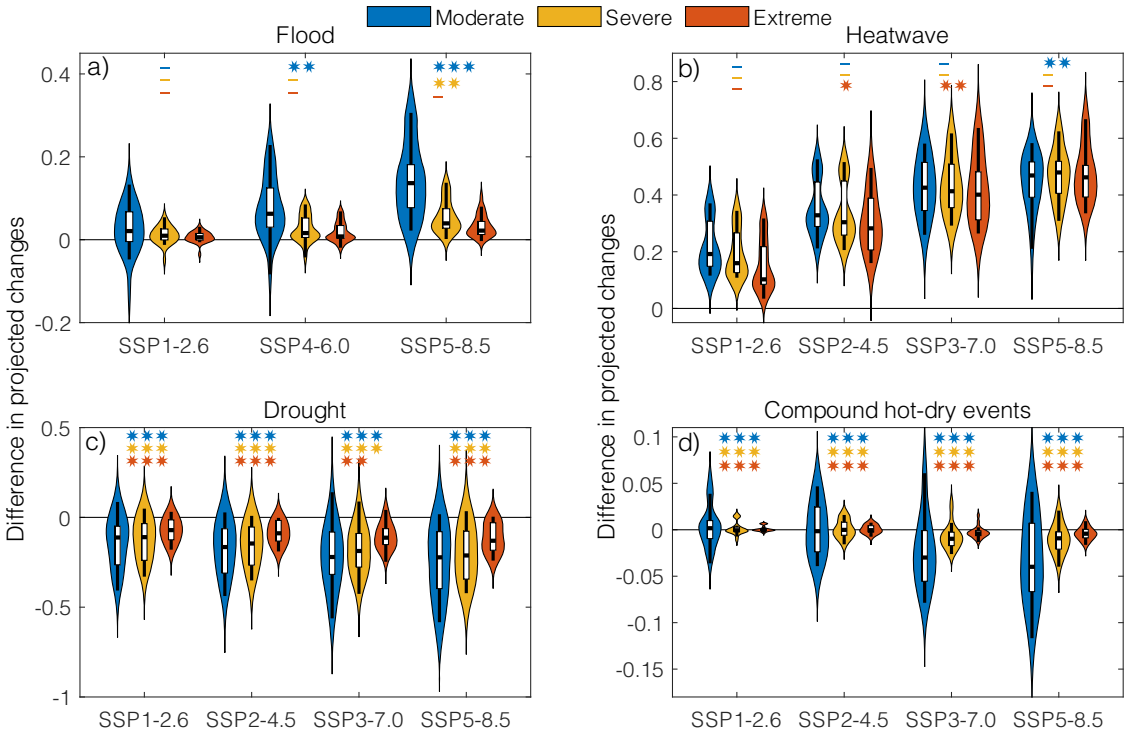

Fig. 5 | Difference in projected changes in the occurrence probability of extreme events of different severities between low- and high-income countries across various future scenarios. Positive values indicate larger changes in low-income countries, while negative values represent larger changes in high-income countries. Violin plots depict the ensemble probability density, with $n = 28$, 18, 22, and 22 ensemble members used for **a** flood, **b** heatwave, **c** drought, and **d** compound events, respectively. Box plots within the violins show the median (horizontal black line), the interquartile range (IQR) from the 25th to 75th percentile (box), and whiskers extending to the most extreme data points within 1.5 × IQR from the box. Statistical significance was calculated using the two-sided Wilcoxon rank-sum test, with "✱✱✱," "✱✱," and "✱" indicating significant inequality at 1%, 5%, and 10% levels, respectively, while "–" indicates no significance.

contribution of population growth. The impact of climate change on more extreme events is well-documented[56–58].

Previous research has highlighted that compound extreme events often lead to more severe ecological and socioeconomic damage than single-hazard events[27,28]. Our findings align with these studies, demonstrating a more extensive and globally distributed population exposure to compound events (Fig. 3). The larger future impact of compound extremes compared to single events is driven by two primary factors: (1) the concurrent intensification of drought and heatwave events (Fig. 1 and Supplementary Fig. 3), and (2) a strengthened relationship between temperature and hydrological cycle variables, fueled by amplified land-atmosphere feedbacks and shifts in shared drivers such as large-scale atmospheric circulation patterns[59–61]. However, a key insight from our analysis is that, while both projected single and compound events exhibit population exposure inequality, this inequality is notably larger for single events (Fig. 2). This finding is important because it reveals that the impacts of single events, such as droughts, are larger in low-income countries. In contrast, compound events, like hot-dry events, tend to have a more geographically widespread impact, reducing the relative disparity in exposure between low- and high-income countries.

Our results show that the highest levels of inequality in human exposure to extreme events between low- and high-income countries occur under the SSP3 and SSP4 scenarios, while the lowest inequality is observed under SSP1. This inequality is primarily driven by differences in population growth, which vary markedly across SSP scenarios due to differing assumptions about fertility, mortality, migration, and education trends[62]. In SSP3, the stark difference in fertility rates is the main driver of inequality between low- and high-income countries. Low-income countries experience high fertility rates, leading to rapid population growth and increasing the number of people exposed to climate extremes. In contrast, high-income countries maintain low fertility rates, resulting in much slower population growth. Other factors—such as high mortality, low education, and low migration—remain similar across both groups, emphasizing fertility as the dominant factor[44]. Similarly, in SSP4, inequality is exacerbated by disparities in access to education and resources, which reinforce differences in fertility rates between low- and high-income countries. High-income countries benefit from advanced education systems and healthcare infrastructure, enabling low fertility rates and sustained human capital development. Low-income countries, however, face limited access to such resources, resulting in high fertility rates and slower demographic transitions. These conditions intensify population growth in low-income countries, increasing exposure to climate extremes and widening the inequality gap[44]. By comparison, SSP1 represents a sustainable pathway where investments in education, healthcare, and equitable economic growth accelerate the demographic transition in low-income countries[44]. These measures reduce fertility rates and population growth, leading to more balanced exposure trends between low- and high-income countries. Consequently, SSP1 exhibits the lowest levels of inequality in human exposure to extreme events.

While climate change mitigation and adaptation strategies remain essential, our findings underscore the critical need to integrate population growth management into adaptation planning, particularly in low-income countries. Investments in education, healthcare, and family planning can substantially curb future population growth, reducing the number of people exposed to climate extremes and narrowing the inequality gap. Such measures, which have received relatively less attention in adaptation policies[63], are crucial for building sustainable and equitable resilience to climate change impacts. International collaboration to support these efforts in low-income regions

https://doi.org/10.1038/s41467-025-63385-3

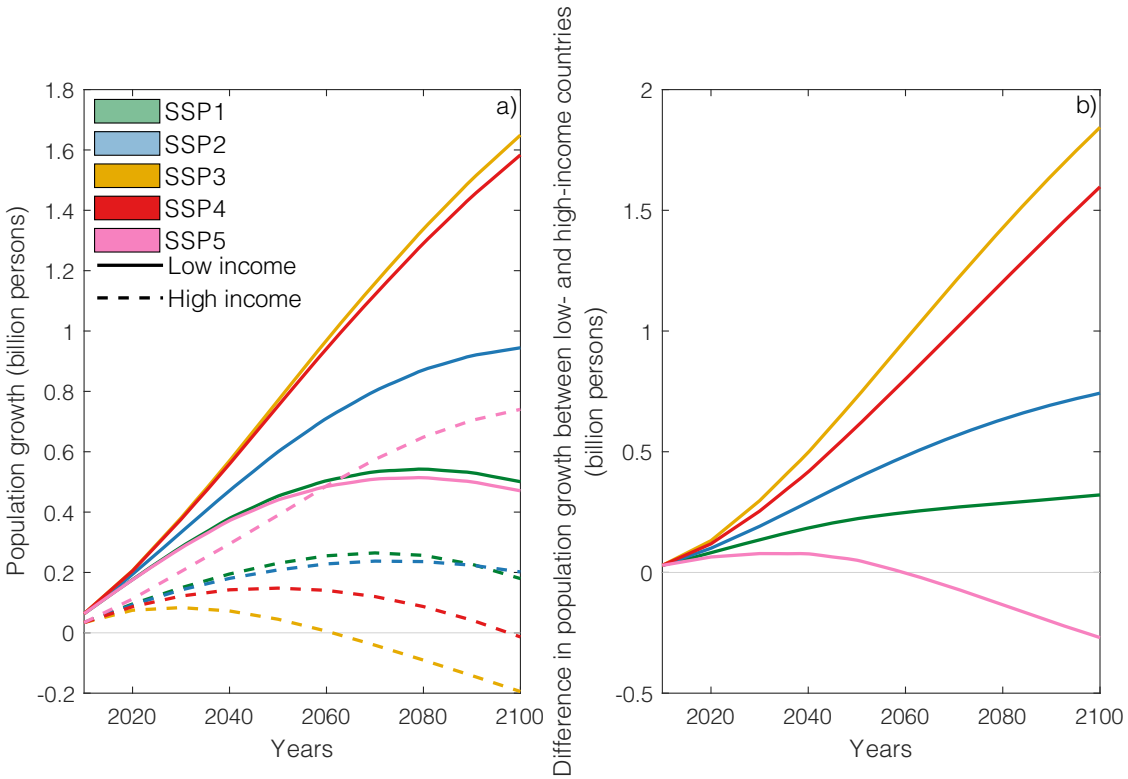

Fig. 6 | Diverging population growth by income group under different SSP scenarios. a Trajectories of population growth for low- and high-income countries through 2100 under each SSP. **b** Population growth inequality, with positive values indicating higher population growth in low-income countries. The differences in population growth between high- and low-income countries across all scenarios are statistically significant at the 1% level, based on the two-sided Wilcoxon rank-sum test.

is imperative for addressing exposure disparities and mitigating the effects of future extreme events.

While our study provides valuable insights into the broader exposure inequalities between low- and high-income countries, it also underscores the need for further research. We used a static income classification based on 2022 GNI per capita. However, this approach does not account for economic mobility over time, as countries may transition between income categories due to sustained growth or economic downturns. Incorporating probabilistic income reclassification in future work—for example, using GDP growth projections—could provide a more nuanced representation of population exposure inequality between low- and high-income countries by accounting for their potential economic transitions. Furthermore, vulnerability is not uniform within income categories, as it is influenced by factors beyond income level, such as economic diversity, the quality of institutions and government policies (e.g., climate governance and migration management), the robustness of infrastructure (e.g., healthcare systems and disaster preparedness, and climate-resilient urban planning), and historical context (e.g., colonial legacies and past exploitation). Internal inequalities also exist within countries. In low-income nations, high population growth drives substantial urbanization, leading many to settle in informal settlements on the outskirts of major cities. These low-income urban residents often live in overcrowded and hazard-prone areas, such as flood-prone zones[64], exacerbating health inequalities and vulnerabilities, including limited access to healthcare and inadequate infrastructure[65,66]. Many of these development and settlement patterns are still shaped by colonial legacies, which were structured around maximizing resource extraction rather than supporting locally adapted, sustainable growth. As a result, urban expansion often ignores traditional environmental knowledge and reinforces spatial and social inequalities. Rapid rural-to-urban migration can also diminish local knowledge and capacity to manage risks[67], making slums particularly vulnerable to climate-related hazards and leading to severe consequences such as malnutrition and disease outbreaks[68]. Conversely, internal inequalities in wealthier countries may be exacerbated by migration from lower-income regions due to climate change[69,70], potentially contributing to socioeconomic segregation within affluent cities. Future work could integrate high-resolution datasets to develop subnational projections that capture these critical gradients in vulnerability.

Our analysis focused on population exposure to extreme events. Future research should explore additional dimensions of social inequality beyond exposure, such as how factors like age, gender, and education affect vulnerability. For example, the elderly in low- and middle-income countries, projected to account for nearly 80% of the global elderly population[71], are expected to face increased exposure risk due to inadequate healthcare and urbanization effects[72]. Addressing these aspects will be crucial for developing targeted strategies that enhance resilience and ensure equitable disaster risk management. Nonetheless, our study provides a thorough assessment of inequality in exposure to multiple extreme events of varying severities under different future scenarios, setting the stage for future research to refine and address these complex challenges.

Methods

Data

For drought, heatwave, and compound hot-dry events, GCMs data from the CMIP6 High-Resolution Model Intercomparison Project (HighResMIP) were used. The incorporated variables include precipitation flux (including both liquid and solid phases), total runoff (which includes drainage through the base of the soil model), total soil moisture content (summed water in all phases across all soil layers), humidity, atmospheric pressure, and near-surface air temperature. We analyzed CMIP6 GCM data for both historical simulations and four

future tier 1 scenarios (SSP1-2.6, SSP2-4.5, SSP3-7.0, and SSP5-8.5) covering the period 1971–2100. The CMIP6 GCMs used for drought, heatwave, and compound hot-dry events are listed in Supplementary Table 1. We adopted the "ensemble of opportunity" approach, including all available CMIP6 models that met our data requirements for specific climate extreme variables. Our preliminary sensitivity analysis shows that our conclusions are robust to the inclusion/exclusion of subsets of GCMs. The CMIP6 models have been extensively evaluated for their performance in simulating heatwaves[73,74], droughts[75,76], and compound hot-dry events[77,78] in prior studies.

For flood analysis, we used the Inter-Sectoral Impact Model Intercomparison Project (ISIMIP) GHMs data due to its specialized focus on hydrological processes, higher resolution, and calibration with observed data[79]. We obtained daily discharge simulations from seven ISIMIP GHMs. These GHMs were driven by climate projections from four CMIP5 GCMs (GFDL-ESM2M, HadGEM2-ES, IPSL-CM5A-LR, and MIROC5) under RCP2.6, RCP6.0, and RCP8.5. The GHMs included CLM4.5[30], H08[31], JULES-W1[32], LPJmL[33], MATSIRO[34], ORCHIDEE[35], and WaterGAP2[36]. Each GHM was driven by three state-of-the-art, observation-based historical climate datasets: GSWP3[37], PGFv2[38], and WFD/WFDEI[39]. Further details on the hydrological processes represented in the GHMs used, including water flows, storage compartments, and human water use sectors, can be found in Telteu et al.[80]. The ISIMIP GHMs have been evaluated for their performance in flood simulations in several previous studies[81,82].

For exposure analysis, we utilized annual changes in population data at a spatial resolution of 0.5° × 0.5° for historical and future periods (2005 and 2085). The gridded population dataset included historical population from the HYDE3.2 database[83], and future population data derived by scaling up the 2010 Gridded Population of the World (GPWv3) dataset (available at http://sedac.ciesin.columbia.edu/data/collection/gpw-v3) using national decadal population projections based on SSP1, SSP2, SSP3, and SSP5[62]. The 2022 GNI per capita classifications of countries were obtained from World Bank datasets.

Quantification of extreme events

Flood. For the flood analysis, we derived block maxima time series of daily discharge for each grid cell for both historical (1971–2000) and future (2070–2099) periods. The generalized extreme value distribution (GEV), as the best-fitted distribution for block maxima series[84], was applied to fit the discharge block maxima. We then calculated flood return periods and, to quantify climate change impacts, determined the future return period of the historical extreme discharge for $T = 10$, 50, and 100 years as follows[56]:

$$T = \frac{1}{1-\psi(I_T)} \tag{1}$$

where I_T represents the discharge for the return period T, and $\psi(I_T)$ is expressed as:

$$\psi(I_T) = \exp\left\{-\left[1+\xi\left(\frac{I_T-\mu}{\sigma}\right)\right]^{-\frac{1}{\xi}}\right\} \tag{2}$$

Here, μ, σ, and ξ denote the location, scale, and shape parameters of the GEV distribution, respectively. The function ψ was defined for $1+\xi\left(\frac{I_T-\mu}{\sigma}\right) > 0$, with ψ being either 0 or 1 elsewhere. The value I_T was determined by the following equation:

$$I_T = \begin{cases} \mu + \frac{\sigma}{\xi}\left\{1-\left[-\ln\left(1-\frac{1}{T}\right)\right]^{\xi}\right\} & if \quad \xi \neq 0 \\ \mu - \sigma\ln\left[-\ln\left(1-\frac{1}{T}\right)\right] & if \quad \xi = 0 \end{cases} \tag{3}$$

The probability of floods was calculated based on return periods, with return periods of $T = 10$, 50, and 100 years corresponding to moderate, severe, and extreme floods, respectively. Our initial analysis indicates that the results are not affected by extrapolation, which was used to estimate the 50- and 100-year flood events.

Heatwave. Extreme heat negatively impacts human health by worsening preexisting medical conditions and leading to higher mortality rates[85]. The combination of air temperature and humidity is essential in determining environmental conditions conducive to heat stress on human health. Humidity decreases the efficiency of evaporative cooling, the primary process by which the human body dissipates heat. When combined with high air temperature, this can pose a serious threat to human health and even life safety[74]. To quantify heatwaves, we used the wet-bulb globe temperature (T_{WBG}), defined as a weighted mean of wet-bulb temperature (T_{WB}) and near-surface air temperature (T) as follows:

$$T_{WBG} = 0.7T_{WB} + 0.3T \tag{4}$$

T_{WB} is calculated using temperature, relative humidity, and pressure through the equivalent potential temperature[86]. Relative humidity was derived from specific humidity, surface pressure, and temperature using the improved Magnus formula approximation[87]. We defined the probability of heatwaves for each model grid cell as the fraction of days where T_{WBG} exceeds the 90th, 95th, and 99th percentiles of T_{WBG} from the historical period 1971–2000. These thresholds correspond to moderate, severe, and extreme heatwaves, respectively.

Drought. Climate change impacts on drought are more accurately assessed by directly examining climate model outputs (e.g., soil moisture and runoff), which explicitly represent the core physical processes often missing in simpler index-based impact models (e.g., SPI and SPEI)[88,89]. These simpler indices tend to underestimate the impacts of climate change in drought hotspots, particularly in dry regions[90]. To capture the interactions between different hydrological variables, we employed the Multivariate Standardized Drought Index[91] (MSDI), a method increasingly used in assessing climate change impacts on global droughts[58,92]. The MSDI was calculated for each grid cell in the CMIP6 GCMs by analyzing the joint distribution of precipitation, runoff, and soil moisture using copula functions. To calculate the MSDI, the copula (C) of the continuous random variables of precipitation, runoff, and soil moisture (u_1, u_2, u_3) was defined as:

$$C(u_1, u_2, u_3) = P(U_1 \le u_1, U_2 \le u_2, U_3 \le u_3) \tag{5}$$

where $(U_1, U_2, U_3) = (F_{X_1}, F_{X_2}, F_{X_3})$, and F_{X_1}, F_{X_2}, and F_{X_3} are the marginal cumulative distribution functions of X_1, X_2, and X_3. Three-dimensional nested copulas with two nesting levels[93] were used by embedding copulas within each other:

$$C(u) = C_0(u_1, C_1(u_2, u_3)) = P, u \in [0,1]^3 \tag{6}$$

where C_k is generated by the generator ψ_k, $k \in [0,1]$ and P is the joint probability, which is then standardized into MSDI using the standard normal distribution function ($MSDI = \varphi^{-1}(p)$).

Drought events were identified when the MSDI dropped below designated thresholds. Specifically, thresholds of −1, −1.5, and −2 were set to indicate the upper limits of moderate, severe, and extreme droughts, respectively, in line with established drought classification standards[58]. The probability of drought occurrence for both historical (1971–2000) and future (2071–2100) periods was determined by calculating the number of drought months relative to the total number of months in each period.

Compound hot-dry event. To account for the interactions between different hydrological variables and the importance of considering various water balance components when studying compound hot-dry extremes[94], we quantified compound hot-dry events by calculating the joint probability between the MSDI and the Standardized Temperature Index[27] using bivariate copulas. We employed the Gaussian, Gumbel, and Clayton copula functions to capture different dependencies between hot and dry events. The Gaussian copula models general symmetric dependence, providing a broad view of the joint behavior of these variables. The Gumbel copula focuses on upper tail dependence, making it ideal for analyzing extreme events where severe droughts and heatwaves coincide. The Clayton copula captures lower tail dependence, allowing us to understand the co-occurrence of milder events[95]. As the differences between the results of various copulas were negligible, only the results from the Gaussian copula are included in the paper. By applying the standard normal distribution to transform the remapped joint probability obtained from the copula functions, we derived the Standardized Compound Hot-Dry Event Index (HDI), following the principles of the MSDI. The probability of occurrence for historical (1971–2000) and future (2071–2100) periods was determined by the ratio of instances with a compound event to the total number of months in each period. A compound hot-dry event was defined as occurring whenever the HDI fell below thresholds of −0.8, −1.3, and −1.6, corresponding to moderate, severe, and extreme events[96], respectively.

Estimation of exposure inequality

After calculating the probability of extreme events, we determined the population exposure to these events at each model grid cell for both historical and future periods. This was done by multiplying the population by the probability of the events at each grid cell. The resulting gridded exposure values were then aggregated to the country level. To assess the changes in population exposure under different SSP scenarios, the difference in exposure between historical and future periods was calculated. The median exposure for each of the four World Bank income groups (low, lower-middle, upper-middle, and high) was then determined, with income group classification based on the 2022 GNI per capita, calculated using the World Bank Atlas method. The exposure inequality was defined as the difference in projected changes in population exposure between low and high-income countries. A positive exposure inequality indicates higher population exposure in low-income countries compared to high-income countries. To test the significance of this inequality, the non-parametric Wilcoxon rank-sum test was used to compare the exposure changes between low- and high-income countries, with the null hypothesis being that the distributions of exposure changes are identical in both groups.

Drivers of exposure inequality

The analysis of exposure to different types of extremes was conducted for various combinations of driving physical (climate change) and socioeconomic (population growth) processes to understand their contributions to exposure inequality. The following three combinations were considered:

- Static climate combined with a dynamic population, which highlights the exposure inequality driven exclusively by population growth.
- Dynamic climate combined with a static population, which reflects the exposure inequality resulting solely from climate change.
- Dynamic climate and dynamic population, which assesses the combined impact of future climate and population changes on exposure inequality.

The relative contributions of climate change (ρ_{CC}) and population growth (ρ_{pop}) were quantified as follows:

$$\rho_{CC} = 100 \times \left(\frac{E_{ineq}(CC)}{\left|E_{ineq}(CC)\right| + \left|E_{ineq}(pop)\right|} \right) \tag{7a}$$

$$\rho_{pop} = 100 \times \left(\frac{E_{ineq}(pop)}{\left|E_{ineq}(CC)\right| + \left|E_{ineq}(pop)\right|} \right) \tag{7b}$$

where $E_{ineq}(CC)$ and $E_{ineq}(pop)$ denote the exposure inequality arising from climate dynamics and population dynamics, respectively.

Data availability

The CMIP6 GCM data used to quantify drought, heatwaves, and compound hot-dry events in this study are available through the Earth System Grid Federation (ESGF) system at: https://esgf-node.ipsl.upmc.fr/projects/cmip6-ipsl/. The daily discharge simulations used to quantify floods were extracted from the ISIMIP portal: https://www.isimip.org/. The population data used to assess population exposure were also obtained from https://www.isimip.org/. The 2022 gross national income (GNI) per capita classifications of countries were retrieved from the World Bank: https://data.worldbank.org/indicator/NY.GNP.ATLS.CD. All data and code required to reproduce the figures are publicly available at: https://zenodo.org/records/15854661.

Code availability

The codes used in this study are available at: https://zenodo.org/records/15854661.

References

1. Tabari, H., Madani, K. & Willems, P. The contribution of anthropogenic influence to more anomalous extreme precipitation in Europe. *Environ. Res. Lett.* **15**, 104077 (2020).
2. Reed, K. A., Wehner, M. F. & Zarzycki, C. M. Attribution of 2020 hurricane season extreme rainfall to human-induced climate change. *Nat. Commun.* **13**, 1905 (2022).
3. Zhou, S., Yu, B. & Zhang, Y. Global concurrent climate extremes exacerbated by anthropogenic climate change. *Sci. Adv.* **9**, eabo1638 (2023).
4. Ahmadalipour, A., Moradkhani, H. & Kumar, M. Mortality risk from heat stress expected to hit poorest nations the hardest. *Clim. Change* **152**, 569–579 (2019).
5. WMO. *Atlas of Mortality and Economic Losses from Weather, Climate and Water Extremes (1970–2019)* WMO-No. 1267 (WMO, 2021).
6. Eckstein, D., Künzel, V. & Schäfer, L. Global climate risk index 2021. Germanwatch e.V. https://www.germanwatch.org/sites/default/files/Global%20Climate%20Risk%20Index%202021_2.pdf (2021).
7. Ahmadalipour, A. & Moradkhani, H. Escalating heat-stress mortality risk due to global warming in the Middle East and North Africa (MENA). *Environ. Int.* **117**, 215–225 (2018).
8. Formetta, G. & Feyen, L. Empirical evidence of declining global vulnerability to climate-related hazards. *Glob. Environ. Change* **57**, 101920 (2019).
9. Gazzotti, P. et al. Persistent inequality in economically optimal climate policies. *Nat. Commun.* **12**, 3421 (2021).
10. Jay, O. et al. Reducing the health effects of hot weather and heat extremes: from personal cooling strategies to green cities. *Lancet* **398**, 709–724 (2021).
11. Callahan, C. W. & Mankin, J. S. Globally unequal effect of extreme heat on economic growth. *Sci. Adv.* **8**, eadd3726 (2022).

12. McElroy, S., Ilango, S., Dimitrova, A., Gershunov, A. & Benmarhnia, T. Extreme heat, preterm birth, and stillbirth: a global analysis across 14 lower-middle income countries. *Environ. Int.* **158**, 106902 (2022).
13. Wing, O. E. J. et al. Inequitable patterns of US flood risk in the Anthropocene. *Nat. Clim. Change* **12**, 156–162 (2022).
14. Hallegatte, S., Fay, M. & Barbier, E. B. Poverty and climate change: Introduction. *Environ. Dev. Econ.* **23**, 217–233 (2018).
15. Masood, E., Tollefson, J. & Irwin, A. COP27 climate talks: What succeeded, what failed and what's next. *Nature* **612**, 16–17 (2022).
16. Ahmadalipour, A., Moradkhani, H., Castelletti, A. & Magliocca, N. Future drought risk in Africa: integrating vulnerability, climate change, and population growth. *Sci. Total Environ.* **662**, 672–686 (2019).
17. Hosseinzadehtalaei, P., Termonia, P. & Tabari, H. Projected changes in compound hot-dry events depend on the dry indicator considered. *Commun. Earth Environ.* **5**, 220 (2024).
18. Fischer, E. M., Sippel, S. & Knutti, R. Increasing probability of record-shattering climate extremes. *Nat. Clim. Change* **11**, 689–695 (2021).
19. Hosseinzadehtalaei, P., Van Schaeybroeck, B., Termonia, P. & Tabari, H. Identical hierarchy of physical drought types for climate change signals and uncertainty. *Weather Clim. Extrem.* **41**, 100573 (2023).
20. Batibeniz, F., Hauser, M. & Seneviratne, S. I. Countries most exposed to individual and concurrent extremes and near-permanent extreme conditions at different global warming levels. *Earth Syst. Dyn.* **14**, 485–505 (2023).
21. Swain, D. L., Langenbrunner, B., Neelin, J. D. & Hall, A. Increasing precipitation volatility in twenty-first-century California. *Nat. Clim. Change* **8**, 427–433 (2018).
22. Zhang, B., Wang, S., Zscheischler, J. & Moradkhani, H. Higher exposure of poorer people to emerging weather whiplash in a warmer world. *Geophys. Res. Lett.* **50**, e2023GL105640 (2023).
23. Harrington, L. J. et al. Poorest countries experience earlier anthropogenic emergence of daily temperature extremes. *Environ. Res. Lett.* **11**, 055007 (2016).
24. Alizadeh, M. R. et al. Increasing heat-stress inequality in a warming climate. *Earth's Future* **10**, e2021EF002488 (2022).
25. Wang, Y. et al. Global future population exposure to heatwaves. *Environ. Int.* **178**, 108049 (2023).
26. Winsemius, H. C. et al. Disaster risk, climate change, and poverty: assessing the global exposure of poor people to floods and droughts. *Environ. Dev. Econ.* **23**, 328–348 (2018).
27. Zscheischler, J. et al. Impact of large-scale climate extremes on biospheric carbon fluxes: an intercomparison based on MsTMIP data. *Glob. Biogeochem. Cycles* **28**, 585–600 (2014).
28. Tabari, H. & Willems, P. Global risk assessment of compound hot-dry events in the context of future climate change and socio-economic factors. *npj Clim. Atmos. Sci.* **6**, 74 (2023).
29. Eyring, V. et al. Overview of the Coupled Model Intercomparison Project Phase 6 (CMIP6) experimental design and organization. *Geosci. Model Dev.* **9**, 1937–1958 (2016).
30. Lawrence, D. M. et al. Parameterization improvements and functional and structural advances in version 4 of the Community Land Model. *J. Adv. Model. Earth Syst.* **3**, M03001 (2011).
31. Hanasaki, N. et al. An integrated model for the assessment of global water resources–Part 1: model description and input meteorological forcing. *Hydrol. Earth Syst. Sci.* **12**, 1007–1025 (2008).
32. Best, M. J. et al. The Joint UK Land Environment Simulator (JULES), model description–Part 1: energy and water fluxes. *Geosci. Model Dev.* **4**, 677–699 (2011).
33. Bondeau, A. et al. Modelling the role of agriculture for the 20th century global terrestrial carbon balance. *Glob. Change Biol.* **13**, 679–706 (2007).
34. Takata, K., Emori, S. & Watanabe, T. Development of the minimal advanced treatments of surface interaction and runoff. *Glob. Planet. Change* **38**, 209–222 (2003).
35. Guimberteau, M. et al. Testing conceptual and physically based soil hydrology schemes against observations for the Amazon Basin. *Geosci. Model Dev.* **7**, 1115–1136 (2014).
36. Mueller Schmied, H. et al. Variations of global and continental water balance components as impacted by climate forcing uncertainty and human water use. *Hydrol. Earth Syst. Sci.* **20**, 2877–2898 (2016).
37. Dirmeyer, P. A. et al. GSWP-2: Multimodel analysis and implications for our perception of the land surface. *Bull. Am. Meteorol. Soc.* **87**, 1381–1398 (2006).
38. Sheffield, J., Goteti, G. & Wood, E. F. Development of a 50-year high-resolution global dataset of meteorological forcings for land surface modeling. *J. Clim.* **19**, 3088–3111 (2006).
39. Weedon, G. P. et al. The WFDEI meteorological forcing data set: WATCH Forcing Data methodology applied to ERA-Interim reanalysis data. *Water Resour. Res.* **50**, 7505–7514 (2014).
40. O'Neill, B. C. et al. A new scenario framework for climate change research: the concept of shared socioeconomic pathways. *Clim. Change* **122**, 387–400 (2014).
41. Riahi, K. et al. The Shared Socioeconomic Pathways and their energy, land use, and greenhouse gas emissions implications: an overview. *Glob. Environ. Chang.* **42**, 153–168 (2017).
42. Diffenbaugh, N. S., Swain, D. L. & Touma, D. Anthropogenic warming has increased drought risk in California. *Proc. Natl. Acad. Sci. USA* **112**, 3931–3936 (2015).
43. Ridder, N. N. et al. Global hotspots for the occurrence of compound events. *Nat. Commun.* **11**, 5956 (2020).
44. Samir, K. C. & Lutz, W. The human core of the shared socioeconomic pathways: population scenarios by age, sex and level of education for all countries to 2100. *Glob. Environ. Change* **42**, 181–192 (2017).
45. Wang, J. et al. Anthropogenic emissions and urbanization increase risk of compound hot extremes in cities. *Nat. Clim. Change* **11**, 1084–1089 (2021).
46. Zscheischler, J. & Lehner, F. Attributing compound events to anthropogenic climate change. *Bull. Am. Meteorol. Soc.* **103**, E936–E953 (2022).
47. Liu, Y. et al. The patterns, magnitude, and drivers of unprecedented 2022 mega-drought in the Yangtze River Basin, China. *Environ. Res. Lett.* **18**, 114006 (2023).
48. Newman, R. & Noy, I. The global costs of extreme weather that are attributable to climate change. *Nat. Commun.* **14**, 6103 (2023).
49. Tabari, H. Climate change impact on flood and extreme precipitation increases with water availability. *Sci. Rep.* **10**, 13768 (2020).
50. Naumann, G., Cammalleri, C., Mentaschi, L. & Feyen, L. Increased economic drought impacts in Europe with anthropogenic warming. *Nat. Clim. Change* **11**, 485–491 (2021).
51. Ghanbari, M., Arabi, M., Georgescu, M. & Broadbent, A. M. The role of climate change and urban development on compound dry-hot extremes across US cities. *Nat. Commun.* **14**, 3509 (2023).
52. Tabari, H., Hosseinzadehtalaei, P., Thiery, W. & Willems, P. Amplified drought and flood risk under future socioeconomic and climatic change. *Earth's Future* **9**, e2021EF002295 (2021).
53. Hasegawa, T. et al. Extreme climate events increase risk of global food insecurity and adaptation needs. *Nat. Food* **2**, 587–595 (2021).
54. Carrão, H., Naumann, G. & Barbosa, P. Mapping global patterns of drought risk: an empirical framework based on sub-national estimates of hazard, exposure and vulnerability. *Glob. Environ. Change* **39**, 108–124 (2016).
55. Vollset, S. E. et al. Fertility, mortality, migration, and population scenarios for 195 countries and territories from 2017 to 2100: a forecasting analysis for the Global Burden of Disease Study. *Lancet* **396**, 1285–1306 (2020).

56. Tabari, H. Extreme value analysis dilemma for climate change impact assessment on global flood and extreme precipitation. *J. Hydrol.* **593**, 125932 (2021).
57. Myhre, G. et al. Frequency of extreme precipitation increases extensively with event rareness under global warming. *Sci. Rep.* **9**, 16063 (2019).
58. Tabari, H. & Willems, P. Sustainable development substantially reduces the risk of future drought impacts. *Commun. Earth Environ.* **4**, 180 (2023).
59. Seneviratne, S. I. et al. Investigating soil moisture–climate interactions in a changing climate: a review. *Earth Sci. Rev.* **99**, 125–161 (2010).
60. Kopp, R., Easterling, D. R. & Hall, T. Potential surprises–compound extremes and tipping elements. in *Climate Science Special Report: Fourth National Climate Assessment* (eds Wuebbles, D. W. F. D. J., Hibbard, K. A., Dokken, D. J., Stewart, B. C. & Maycock, T. K.) 411–429 (U.S. Global Change Research Program, 2017).
61. Kornhuber, K. et al. Extreme weather events in early summer 2018 connected by a recurrent hemispheric wave-7 pattern. *Environ. Res. Lett.* **14**, 054002 (2019).
62. Samir, K. C. & Lutz, W. Demographic scenarios by age, sex and education corresponding to the SSP narratives. *Popul. Environ.* **35**, 243–260 (2014).
63. Dodson, J. C., Dérer, P., Cafaro, P. & Götmark, F. Population growth and climate change: addressing the overlooked threat multiplier. *Sci. Total Environ.* **748**, 141346 (2020).
64. Kuddus, M. A., Tynan, E. & McBryde, E. Urbanization: a problem for the rich and the poor?. *Public Health Rev.* **41**, 1–4 (2020).
65. Smith, G. S., Anjum, E., Francis, C., Deanes, L. & Acey, C. Climate change, environmental disasters, and health inequities: the underlying role of structural inequalities. *Curr. Environ. Health Rep.* **9**, 80–89 (2022).
66. Putsoane, T., Bhanye, J. I. & Matamanda, A. Extreme weather events and health inequalities: exploring vulnerability and resilience in marginalized communities. *Dev. Environ. Sci.* **15**, 225–248 (2024).
67. Delica-Willison, Z. & Willison, R. Vulnerability reduction: a task for the vulnerable people themselves. in *Mapping Vulnerability: Disasters, Development and People* (eds Bankoff, G., Frerks, G. & Hilhorst, D.) (Earthscan Routledge, 2004).
68. Mirza, M. M. Q. Climate change and extreme weather events: can developing countries adapt?. *Clim. Policy* **3**, 233–248 (2003).
69. Alvarez, J. L. C., & Rossi-Hansberg, E. The economic geography of global warming. National Bureau of Economic Research, NBER Working Paper Series, Working paper No. 28466 (2021).
70. Avtar, R., Blickle, K., Chakrabarti, R., Janakiraman, J. & Pinkovskiy, M. Understanding the linkages between climate change and inequality in the United States. *Econ. Policy Rev.* **29**, 1–39 (2023).
71. Rudnicka, E. et al. The World Health Organization (WHO) approach to healthy ageing. *Maturitas* **139**, 6–11 (2020).
72. Chen, M. et al. Rising vulnerability of compound risk inequality to ageing and extreme heatwave exposure in global cities. *npj Urban Sustain* **3**, 38 (2023).
73. Hirsch, A. L., Ridder, N. N., Perkins-Kirkpatrick, S. E. & Ukkola, A. CMIP6 MultiModel evaluation of present-day heatwave attributes. *Geophys. Res. Lett.* **48**, e2021GL095161 (2021).
74. Chen, X. et al. Changes in global and regional characteristics of heat stress waves in the 21st century. *Earth's Future* **8**, e2020EF001636 (2020).
75. Papalexiou, S. M. et al. Probabilistic evaluation of drought in CMIP6 simulations. *Earth's Future* **9**, e2021EF002150 (2021).
76. Ukkola, A. M., De Kauwe, M. G., Roderick, M. L., Abramowitz, G. & Pitman, A. J. Robust future changes in meteorological drought in CMIP6 projections despite uncertainty in precipitation. *Geophys. Res. Lett.* **47**, e2020GL087820 (2020).
77. Zhang, Y., Hao, Z., Zhang, X. & Hao, F. Anthropogenically forced increases in compound dry and hot events at the global and continental scales. *Environ. Res. Lett.* **17**, 024018 (2022).
78. Ridder, N. N., Ukkola, A. M., Pitman, A. J. & Perkins-Kirkpatrick, S. E. Increased occurrence of high impact compound events under climate change. *npj Clim. Atmos. Sci.* **5**, 3 (2022).
79. Frieler, K. et al. Assessing the impacts of 1.5°C global warming–simulation protocol of the Inter-Sectoral Impact Model Intercomparison Project (ISIMIP2b). *Geosci. Model Dev.* **10**, 4321–4345 (2017).
80. Telteu, C. E. et al. Understanding each other's models: an introduction and a standard representation of 16 global water models to support intercomparison, improvement, and communication. *Geosci. Model Dev.* **14**, 3843–3878 (2021).
81. Mester, B., Willner, S. N., Frieler, K. & Schewe, J. Evaluation of river flood extent simulated with multiple global hydrological models and climate forcings. *Environ. Res. Let.* **16**, 094010 (2021).
82. Yang, T. et al. Evaluation and machine learning improvement of global hydrological model-based flood simulations. *Environ. Res. Let.* **14**, 114027 (2019).
83. Klein Goldewijk, K., Beusen, A., Doelman, J. & Stehfest, E. Anthropogenic land use estimates for the Holocene–HYDE 3.2. *Earth Syst. Sci. Data* **9**, 927–953 (2017).
84. Coles, S. *An Introduction to Statistical Modeling of Extreme Values* (Springer, 2001).
85. Keellings, D. & Moradkhani, H. Spatiotemporal evolution of heat wave severity and coverage across the United States. *Geophys. Res. Lett.* **47**, e2020GL087097 (2020).
86. Schwingshackl, C., Sillmann, J., Vicedo-Cabrera, A. M., Sandstad, M. & Aunan, K. Heat stress indicators in CMIP6: estimating future trends and exceedances of impact-relevant thresholds. *Earth's Future* **9**, e2020EF001885 (2021).
87. Alduchov, O. A. & Eskridge, R. E. Improved Magnus form approximation of saturation vapor pressure. *J. Appl. Meteorol.* **35**, 601–609 (1996).
88. Milly, P. C. & Dunne, K. A. Potential evapotranspiration and continental drying. *Nat. Clim. Change* **6**, 946–949 (2016).
89. Greve, P., Roderick, M. L., Ukkola, A. M. & Wada, Y. The aridity index under global warming. *Environ. Res. Lett.* **14**, 124006 (2019).
90. Hosseinzadehtalaei, P., Ishadi, N. K., Tabari, H. & Willems, P. Climate change impact assessment on pluvial flooding using a distribution-based bias correction of regional climate model simulations. *J. Hydrol.* **598**, 126239 (2021).
91. Hao, Z. & AghaKouchak, A. Multivariate standardized drought index: a parametric multi-index model. *Adv. Water Resour.* **57**, 12–18 (2013).
92. Adeyeri, O. E. et al. Multivariate drought monitoring, propagation, and projection using bias-corrected general circulation models. *Earth's Future* **11**, e2022EF003303 (2023).
93. Tabari, H. & Willems, P. Trivariate analysis of changes in drought characteristics in the CMIP6 multimodel ensemble at global warming levels of 1.5, 2, and 3 °C. *J. Clim.* **35**, 5823–5837 (2022).
94. Jha, S., Gudmundsson, L. & Seneviratne, S. I. Partitioning the uncertainties in compound hot and dry precipitation, soil moisture, and runoff extremes projections in CMIP6. *Earth's Future* **11**, e2022EF003315 (2023).
95. Ribeiro, A. F., Russo, A., Gouveia, C. M. & Pires, C. A. Drought-related hot summers: a joint probability analysis in the Iberian Peninsula. *Weather Clim. Extrem.* **30**, 100279 (2020).
96. Wu, X., Hao, Z., Zhang, X., Li, C. & Hao, F. Evaluation of severity changes of compound dry and hot events in China based on a multivariate multi-index approach. *J. Hydrol.* **583**, 124580 (2020).

Acknowledgements
We gratefully acknowledge the support from the Research Foundation—Flanders (FWO) (grant number: 1255423N), the Horizon Europe project SCEWERO (project ID: 101159497), and the Chinese Academy of Sciences President's International Fellowship Initiative (Grant Nos. 2025PVA0129 and 2025PVB0120). We also thank the World Climate Research Programme (WCRP) for providing CMIP6 GCM data, and the Inter-Sectoral Impact Model Intercomparison Project (ISIMIP) for the global hydrological model and population data.

Author contributions
P.H. and H.T. conceived the study, designed the framework, and performed the analysis. P.H. prepared the first draft of the manuscript. P.T. and H.T. supervised the study and secured its funding. H.M. and R.H. provided critical feedback on the analysis and results. All authors reviewed, commented on, and edited the manuscript.

Competing interests
The authors declare no competing interests.

Additional information
Supplementary information The online version contains supplementary material available at https://doi.org/10.1038/s41467-025-63385-3.

Correspondence and requests for materials should be addressed to Parisa Hosseinzadehtalaei or Hossein Tabari.

Peer review information *Nature Communications* thanks Marleen de Ruiter and the other, anonymous, reviewer(s) for their contribution to the peer review of this work. A peer review file is available.

Reprints and permissions information is available at http://www.nature.com/reprints

Publisher's note Springer Nature remains neutral with regard to jurisdictional claims in published maps and institutional affiliations.

Open Access This article is licensed under a Creative Commons Attribution-NonCommercial-NoDerivatives 4.0 International License, which permits any non-commercial use, sharing, distribution and reproduction in any medium or format, as long as you give appropriate credit to the original author(s) and the source, provide a link to the Creative Commons licence, and indicate if you modified the licensed material. You do not have permission under this licence to share adapted material derived from this article or parts of it. The images or other third party material in this article are included in the article's Creative Commons licence, unless indicated otherwise in a credit line to the material. If material is not included in the article's Creative Commons licence and your intended use is not permitted by statutory regulation or exceeds the permitted use, you will need to obtain permission directly from the copyright holder. To view a copy of this licence, visit http://creativecommons.org/licenses/by-nc-nd/4.0/.

© The Author(s) 2025